CELLULAR AUTOMATA AS A MEANS FOR DETECTING INFRARED OBJECTS

STEFAN RIZANOV*, PETER YAKIMOV, DIMITAR NIKOLOV AND BORISLAV GANEV

Department of Electronics, Technical University of Sofia
Bul. „St. Kliment Ohridski" 8, 1000, Sofia, Bulgaria
e-mails: srizanov@tu-sofia.bg, pij@tu-sofia.bg, d_nikolov@tu-sofia.bg, b_ganev@tu-sofia.bg

Abstract. The goal of the present work is to propose a novel cellular automata algorithm for infrared object detection. The algorithm's application is aimed towards computationally limited edge computing sensory modules. Performed is a statistical evaluation of the algorithm's noise resilience through a 3D histogram method. Proposed is a methodology for the optimal choice of the algorithm's fine-tuning parameter values. Proposed is the synthesis of a thermogram dataset based on Perlin/Simplex noise. The algorithm's resilience to apparent temperature modulation was evaluated, with this effect being resultant from physical, optical, and external environmental factors – causing objects to appear hotter or cooler than they actually are.

Keywords: infrared images, object detection, Perlin noise, Simplex noise, temperature modulation

1. INTRODUCTION

Thermal image analysis and automated object detection have attracted significant scientific attention due to their wide applicability in military operations, emergency response systems, pedestrian monitoring, and biomedical diagnostics. With the increasing availability of compact infrared matrix focal plane array (FPA) sensors, their integration into computationally constrained, battery-powered, portable, and IoT edge-computing devices has become a growing area of interest. However, most existing algorithms for infrared object detection are designed for centralized, high-performance systems, such as servers, which process data collected from sensory end-devices using methods primarily derived from machine learning and deep neural networks.

In contrast, our research focuses on developing an infrared object detection and tracking algorithm that can be executed directly on resource-limited edge-computing

*Corresponding author
http://doi.org/10.7546/EngSci.LXII.25.04.07

devices. The resulting method is a fusion-based algorithm that combines gradient thresholding with a cellular automata-inspired pixel similarity identification strategy.

The structure of this paper is as follows: Section 2 provides a concise review of infrared object detection techniques. Section 3 introduces the proposed algorithm and presents its statistical evaluation. To assess performance and noise resilience, we subjected the algorithm to statistical testing by applying synthetic white noise of variable thermal variance to a test image. Noise levels were progressively increased, and three-dimensional histograms were employed to visualize the algorithm's robustness. Additionally, we introduce performance criteria and propose a methodology for parameter fine-tuning to achieve optimal results. Section 4 is centered around the physical phenomenon of apparent thermal modulation and evaluating how resilient the developed algorithm is to it. Finally, Section 5 discusses the proposed methodology of synthesizing thermal images based on Perlin/Simplex noise.

2. INFRARED OBJECT DETECTION

Thermal images typically exhibit low contrast and limited texture information, with blurred object contours [1, 2]. Furthermore, infrared images generally have lower signal-to-noise ratios (SNR) and contain fewer discriminative features [3]. Consequently, many studies rely on multimodal approaches, combining infrared data with additional modalities rather than using infrared imaging alone [1, 4, 5]. The combined problem of multimodal image fusion and object detection has been widely investigated, leading to proposed solutions such as Target-Aware Dual Adversarial Learning (TarDAL) networks and Meta Fusion Embedding (MFE) [5-7].

Previous research has introduced a variety of deep learning-based methods, including Single Shot Detection (SSD), You Only Look Once (YOLO), Fully Convolutional One-Stage (FCOS) detection, Faster R-CNN, Task-Aligned One-Stage Object Detection (TOOD), U-Net, and other algorithmic approaches [3,8,9]. Reported accuracies for some of these methods reach up to 88.69% at a video frame rate of 50 FPS [3]. In addition, multimodal feature fusion networks have been proposed to improve performance in small-object detection tasks [3]. However, the absence of color information in thermal images significantly reduces the detection accuracy of convolutional neural network (CNN) models [2]. To address the limited availability of infrared training datasets, methods such as CycleGAN have been employed to generate synthetic thermal images from visible-spectrum data, thereby augmenting training sets [10]. For mitigating environmental artifacts such as camera jitter and background motion, statistical modeling approaches like the Fuzzy Mixture of Gaussians (Fuzzy MOG) have also been proposed [11].

YOLO, a CNN-based architecture, has been applied in several studies, primarily for nighttime person detection and border surveillance [1, 2, 12, 13]. However, architectures of this type are computationally intensive and thus difficult to implement on resource-constrained edge devices. For example, YOLOv3 contains 106 layers, 75 of which are convolutional [1], making deployment on compact, battery-powered IoT systems challenging without additional energy-harvesting strategies.

Infrared imaging and object detection remain key areas of research with practical applications in pedestrian monitoring, autonomous driving, and search-and-rescue (SAR) robotics [1].

3. DEVELOPED CELLULAR AUTOMATA ALGORITHM

The object recognition module computes an object mask for each captured thermogram and defines which pixels are part of an object. Two Python functions perform this: Image_OBJ_Mask (...) and Quick_OBJ_Mask (...). The function Extract_OBJ_Parameters (...) calculates the object parameters. Figure 1 shows a pseudo-code representation of these three functions.

```
Image_OBJ_Mask (IR_Image, Threshold, Offset):

Create empty 2D array of size(IR_Image)
Extract corner (x,y) gradients
Extract edge (x,y) gradients
Extract internal (x,y) gradients
IF (Extracted_Gradients > Threshold):
   Mark IR_Image Pixels as OBJ_Contour_Pixels
   Add OBJ_Contour_Pixels to OBJ_Mask
min_val = min(OBJ_Contour_Pixels)
Scan IR_Image_Pixels
IF ( Image_Pixel > (min_val - Offset) ):
   Add IR_Image_Pixel to OBJ_Mask

return OBJ_Mask
```

```
Quick_OBJ_Mask (IR_Image):

Calculate: min(IR_Image)
           max(IR_Image)
           avg(IR_Image)
Dynamic_Threshold = min(IR_Image)+
                    ( max(IR_Image) -
                      min(IR_Image)
                    ) / 2

Dynamic_Offset = avg(IR_Image) * 0.02
Image_OBJ_Mask (IR_Image,
                Dynamic_Threshold,
                Dynamic_Offset)

return OBJ_Mask
```

```
Extract_OBJ_Parameters (IR_Image, OBJ_Mask):

Scan OBJ_Mask elements
IF OBJ_Mask element marks OBJ_Pixel :
   Add coresponding IR_Image Pixel to 1D List
Calculate: min(OBJ_Pixels)
           max(OBJ_Pixels)
           avg(OBJ_Pixels)
           median(OBJ_Pixels)

return min, max, avg, median
```

Fig. 1. Pseudo-code representation of the object recognition software functions

The developed automated object recognition software package is based on two complementary techniques: gradient-based contour detection and cellular automata. In the gradient-based contour detection method, each image pixel is evaluated by calculating a set of gradients (temperature differences) relative to its neighboring pixels. Since corner pixels, edge pixels, and internal pixels differ in the number of neighbors, three distinct sub-functions were implemented. After computing these gradients, the software module verifies whether any exceed a predefined threshold. If one or more gradients surpass this threshold, the corresponding pixel is classified as a contour pixel.

This approach is widely applied in image processing because objects in the visible spectrum typically exhibit sharply defined contours, which delineate their shape. Analogously, thermal objects also display distinct shapes, defined by differences in thermal signatures relative to surrounding pixels. While contour detection identifies object boundaries, it does not capture internal pixels, as the latter exhibit nearly uniform thermal distribution and thus yield small gradients with neighboring pixels.

To address this, a cellular automata approach was employed to identify internal object pixels. The procedure begins by locating the contour pixel with the lowest thermal value, which serves as a reference. All pixels with values above this minimum contour pixel are then classified as belonging to the object. This approach is justified by the observation that contour pixels generally have lower temperatures than internal object pixels, owing to surface energy distribution in thermal imagery. The cellular automata mechanism is therefore effective in clustering spatially adjacent pixels with similar thermal values into coherent object regions.

A notable limitation of the combined gradient-cellular automata method in its basic form is its inability to detect *cold spots*. Cold spots are localized non-uniformities within an object, where one or more pixels exhibit abnormally low temperatures compared to their neighbors, while still being part of the object. If the cold spot's temperature falls below that of the minimum contour pixel, such regions remain undetected. To mitigate this issue, a cold-spot detection offset was introduced. This offset is a numerical value (in degrees) that expands the detection criterion: pixels with thermal values higher than the minimum contour pixel minus the offset are also classified as object pixels. The detection threshold can thus be formally expressed as:

$$T_{COLD_{Threshold}} = T_{CONTOUR_{MIN}} - Offset$$

The Image_OBJ_Mask function integrates the described detection steps and outputs an object mask of the same dimensions as the original image. In this mask, pixels identified as belonging to the object are assigned a value of 1.0, while non-object pixels are assigned 0.0.

To simplify object detection, the Quick_OBJ_Mask function was also developed. Unlike Image_OBJ_Mask, this function does not require the operator to manually define a thermal gradient threshold or a cold-spot detection offset. Instead, these values are estimated automatically from the dynamic range of the captured thermal pixels. While this approach proved useful for reducing user input, manual threshold and offset configuration remained necessary for achieving more precise results. The functionality of Quick_OBJ_Mask could be further improved through histogram-based analysis of the thermal image, whereby thresholds and offsets are statistically derived from the distribution of pixel values.

To evaluate the performance of the automated object detection module, several software-based tests were conducted. For these tests, an idealized 8 × 8 pixel image was constructed, containing a thermal object with an embedded cold spot. The object temperature was set to 36.0 °C, the cold-spot pixels to 34.0 °C, and the ambient background pixels to 28.0 °C. These values were selected to emulate real-world biological object detection under moderate, non-elevated ambient temperature conditions.

To assess robustness under noise, artificial noise was introduced into the images. Noise images were generated with the same dimensions as the test image, where noise pixel values were assigned randomly using a dedicated random number generator.

The noise variance parameter, expressed as ± Noise_Variance (°C), was configurable, with higher variance producing greater image distortion.

The first test investigated how varying the gradient threshold (thermal difference) influenced the object detection capabilities of the developed module. The results of this experiment are presented in Fig. 2.

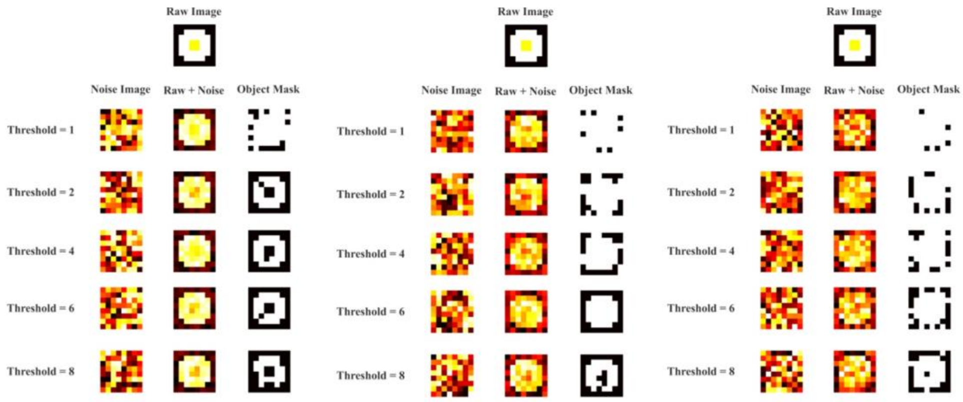

Fig. 2. Object detection at different noise variances with Object detection offset = 0˚C and Noise Variance at respectively ±1˚C, ±3˚C, and ±5˚C

The test results demonstrate that the presence of noise, and particularly its variance, substantially degrades object detection when an inappropriate threshold is selected. The findings indicate that threshold selection must be adapted to the noise variance of the image. Specifically, the threshold value should exceed the thermal noise variance by at least 1 °C to ensure reliable object detection.

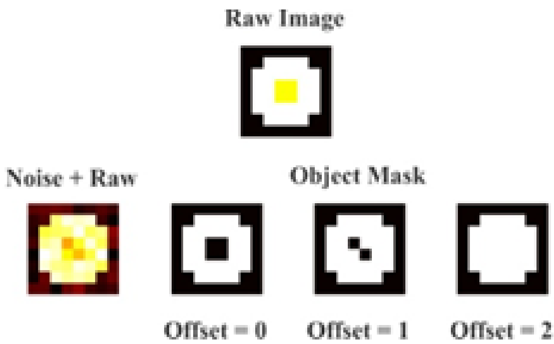

Fig. 3. Cold-spot detection at different offset values,
Noise variance = ±1˚C, thermal gradient threshold = 5˚C

The next test evaluated the performance of the developed cold-spot detection method and examined how the cold-spot offset parameter influences object detection.

The results are presented in Fig. 3. In the test, the cold spot in the original image was 2 °C lower than the surrounding object pixels. A noise variance of ±1 °C was applied, and the thermal gradient threshold was set to 5 °C to ensure reliable object detection.

The results indicate that when the offset value is set to 0.0 °C, the cold spot remains undetected. Proper detection requires selecting the offset parameter in accordance with the temperature difference between the cold spot and neighboring object pixels. When the offset is set to 2 °C, the cold spot is correctly included within the object mask. Increasing the offset further carries the risk of falsely including ambient, non-object pixels in the mask, highlighting the need for careful parameter selection.

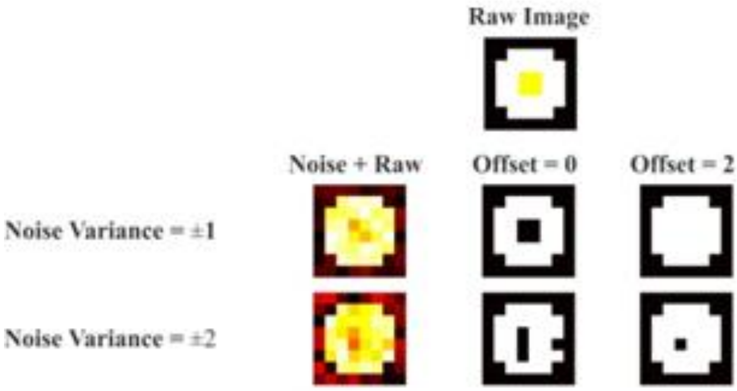

Fig. 4. Cold-spot detection at different noise variances, fixed offsets, thermal gradient threshold = 5˚C.

The subsequent test assessed the robustness of the cold-spot identification methodology against increased thermal noise in the test image. The results, shown in Fig. 4, demonstrate that elevated noise levels degrade the performance of cold-spot detection. In this experiment, the thermal gradient threshold was set to 5.0 °C, and two noise variances were applied: ±1 °C and ±2 °C. The cold-spot offset values were tested at 0.0 °C and 2.0 °C. These findings indicate that the selection of the cold-spot offset must account for the thermal noise variance in the image, with higher noise levels necessitating a proportionally larger offset to maintain detection accuracy.

To further evaluate the algorithm, a statistical assessment was performed using a benchmark thermal image subjected to variable thermal noise. The generated test image, shown in Fig. 5, is an 8 × 8 pixel grid with an ambient background of 28.0 °C. The object contours consist of pixels at 35.0 °C, while thermal non-uniformities were modeled by including a hot ring of pixels at 36.0 °C and a cold spot at 34.0 °C.

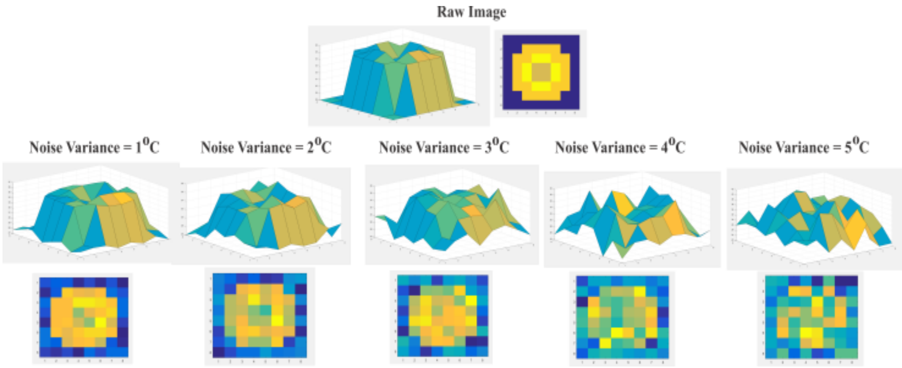

Fig. 5. Statistical test benchmark image.

White thermal noise was applied to the test image, with a thermal variance ranging from ±0.0 °C to ±5.0 °C in incremental steps of 0.2 °C. At each increment, 10,000 thermal images were generated and processed using the developed object detection algorithm. The computed object sizes were then recorded in histograms. The results were visualized as a series of three-dimensional histograms, illustrating the algorithm’s performance across varying thermal noise levels. An example of a generated 3D histogram from these tests is shown in Fig. 6.

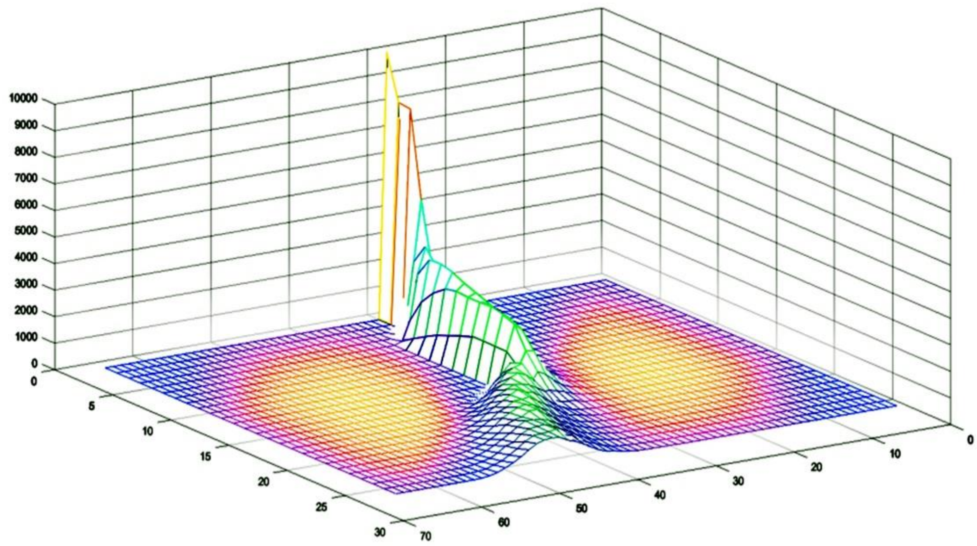

Fig. 6. An example generated 3D histogram.

Because the developed algorithm has two tuning parameters, we wanted to evaluate how these parameters' values influence overall performance. A visual representation of how these tuning parameter values influence object detection is shown in Fig. 7

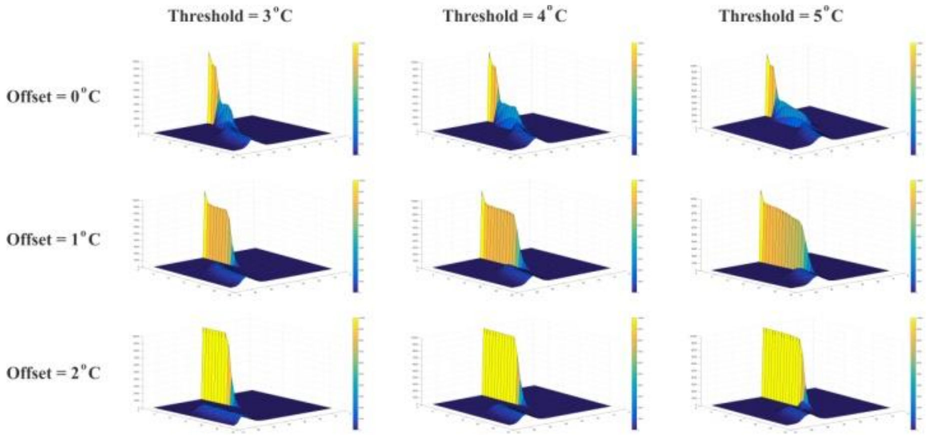

Fig. 7. The influence of tuning parameter values.

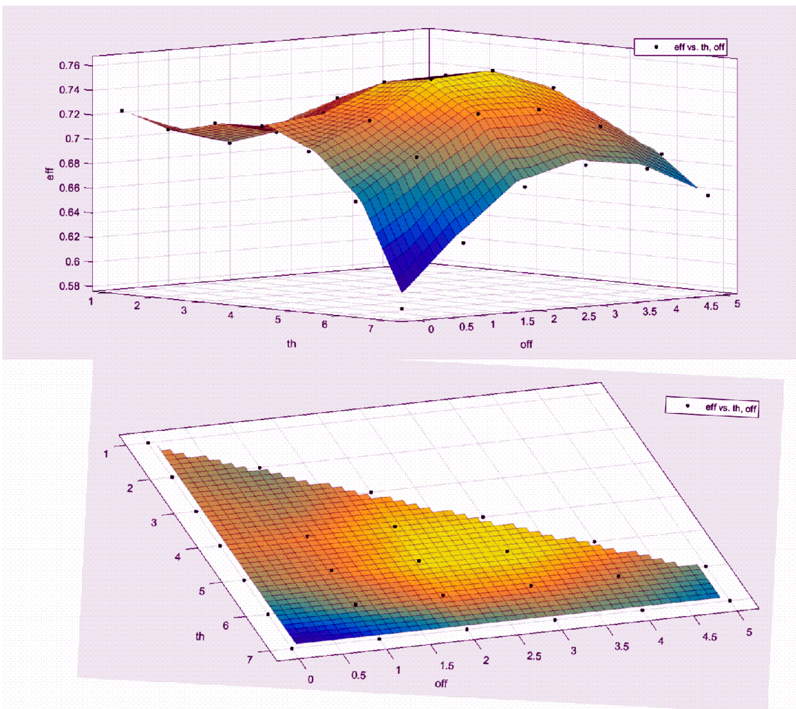

Fig. 8. Tuning parameter optimal selection response surface.

Because proper application of the developed algorithm requires careful selection of tuning parameters, a performance optimization criterion was defined to identify parameter values that maximize object detection performance. The optimization criterion C is defined as:

$$C = \frac{HYST_{Empty\ Pots}}{HYST_{All\ Pots} - N_{Noise\ Steps}} \tag{1}$$

Here, $\mathrm{HYST}_{\mathrm{Empty\ Pots}}$ represents the number of empty bins in the 3D histogram where no objects of the corresponding size were detected during testing $\mathrm{HYST}_{\mathrm{All\ Pots}}$is the total number of histogram bins, and $\mathrm{N}_{\mathrm{Noise\ Steps}}$ denotes the number of incremental noise variance steps. The resulting 3D surface plot of the optimization criterion is shown in Fig. 8. Despite its complex three-dimensional structure, the plot indicates that optimal object detection is achieved with a threshold in the range of 4.0÷6.0 °C and a cold-spot offset between 1.5÷3.5 °C.

From these results, the optimal parameter values can be approximated as:

$$TH_{optimal} = (0.6 \div 0.8) * (Temp_{Object\ Contour} - Temp_{Background}) \tag{2}$$

$$OFF_{optimal} = (1.1 \div 2.7) * (Temp_{Object\ Average} - Temp_{Cold\ Spot}) \tag{3}$$

4. EFFECT OF APPARENT TEMPERATURE MODULATION

An interesting phenomenon often occurs in thermographic imaging called “apparent temperature modulation”. It is caused by complex factors of physical, optical, and external environmental nature, and the resulting effect is that objects appear hotter or cooler than they actually are. Gases and particulates in the air can absorb or emit infrared radiation. IR radiation is partially absorbed by gases such as water vapor, CO_2, or dust in the air. This can reduce the apparent temperature of farther objects. Particles in the air can also scatter IR radiation, which creates diffuse contributions that make some regions appear slightly warmer or cooler. Infrared cameras detect emitted radiation, but they also pick up reflected IR light from surrounding emissive surfaces. A hot wall reflecting on an object can make it appear hotter, while a cold background can reduce apparent temperature. Additionally, variances in thermophysical properties such as object emissivity can result in such an effect. A highly reflective or low-emissivity surface can appear cooler because it emits less infrared radiation. Alternatively, a high-emissivity surface will appear hotter. Surroundings can change the effective emissivity due to reflections, introducing apparent temperature drifts. Temperature modulation can additionally result from non-ideal detectors and IR optics. IR lenses have transmission characteristics that vary with wavelength and angle. These can introduce small modulations of measured temperature across the image. Focal-plane arrays (FPA) in thermal cameras may have pixel-to-pixel variations. Often corrected by calibration, but residual fixed-pattern noise can look like hotter/cooler regions. Thermal cameras integrate radiation over each pixel, which means that near the edges, mixing of object and background temperatures can create apparent modulation. And lastly, environmental factors may also induce this effect when: cooling by air flow locally lowers the surface temperature of objects; direct or reflected solar radiation temporarily increases apparent temperature; nearby hot or cold surfaces emit thermal radiation that is reflected or scattered, modulating the measured temperature.

This effect has not been discussed in past research works, and how it can affect object detection performance. In order to evaluate how resilient the developed algorithm is to temperature modulation, we performed a test where we artificially elevated and decreased the temperature of a generated thermogram. The result from the performed test is shown in Fig. 9. We compared our developed algorithm to threshold-based benchmark algorithms from OpenCV and Scikit-Image.

From the performed test, it can be seen that only the developed algorithm's object detection accuracy is not affected by temperature modulation effects – the OpenCV and Scikit-image algorithms' object masks are deteriorated. The reason behind this is that the developed algorithm is centered around detecting objects based on their contrast in respect to background pixels, whilst the other two algorithms detect objects based on a fixed temperature threshold for semantic segmentation.

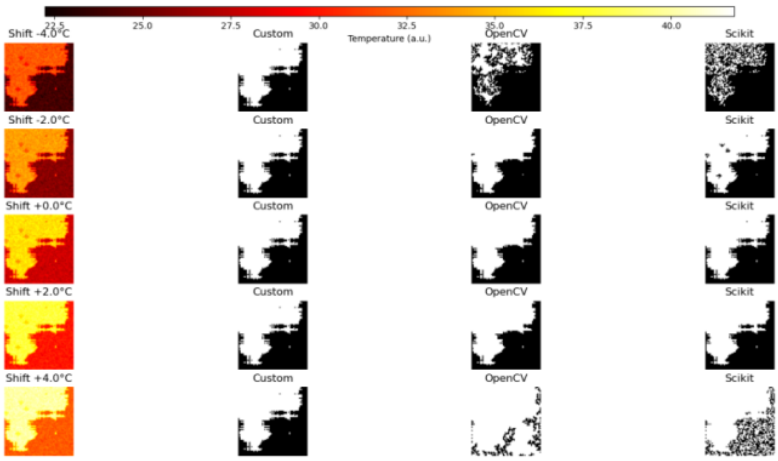

Fig. 9. Temperature modulation resilience test

This means that for the OpenCV and Scikit-image algorithms, when the thermogram has an elevated temperature, the fixed threshold comes close in value to the background temperature, and as a result, non-object noise is included in the object mask. Alternatively, when the thermogram is cooled, then the threshold is closer in value to the maximum temperatures of the object, which results in that some cooler object pixels are not being included in the object mask, and hence the inferred object shape loses its structure.

5. INFRARED IMAGE SYNTHESIS

In order to perform a more comprehensive evaluation of the performance of the algorithm, we need to compare it to existing state-of-the-art object detection algorithms and analyze more complex thermal images. One of the big problems with thermal image datasets is that they are limited in size and scope. This severely limits the testing image set that can be used. One approach is to not rely on ready datasets, but to synthesize thermal images based on specific rules and properties of objects they are observed in the infrared domain.

Within thermal images, objects do not have sharp edges, which is a result of several factors. Objects emit infrared (IR) radiation according to their temperature and emissivity (thermo-physical properties). This emission of radiation is not considered a point source, but it diffuses in space, primarily near the object's edges. This makes boundaries appear blurry. Due to heat conduction and convection, heat can slightly spread into surrounding areas (air or adjacent materials), softening the temperature gradient at edges. There are effects which are also caused by the imaging devices and optics - IR cameras use lenses that have finite resolution, and when light passes through a lens, diffraction causes point sources to blur slightly – a phenomenon called a point spread function (PSF). This effect results in spreading the signal towards the edges. If the camera is slightly out of focus, edge sharpness decreases. Thermal lenses often have a lower depth of field than visible-light lenses. Most thermal sensors have fewer pixels than visible-light cameras. Each pixel measures an average temperature over its area. So, at object edges, a pixel may contain both object and background radiation, giving an intermediate temperature – this is called spatial averaging or partial pixel effect. Infrared radiation is absorbed and scattered by air, humidity, or dust, slightly blurring the image. IR radiation from other sources, such as walls and sun-heated surfaces, can mix with the object's radiation near the edges, potentially softening the apparent boundary.

Taking these properties under consideration, an algorithmic process of synthesizing thermograms must apply some form of edge blurring in order to mimic the properties of objects in the IR domain. Objects cannot be represented as Gaussian blobs, due to the fact that they are very smooth, and even though there is contour blurring, heat diffusion is finite, and thermal objects have fairly abrupt boundaries. For thermal blob generation, our research was focused on Perlin noise [14].

Perlin / Simplex Noise is a technique that generates very natural fractal thermal shapes, which makes it ideal for bio-medical thermal image generation. It combines several layers of noise frequencies and amplitudes, which allow for the construction of objects that have a fractal-like complexity. The method requires a noise generator, and the generated thermograms are unpredictable. The generated 2D noise field (Perlin / Simplex noise) is thresholded at a certain level, which defines which pixels will be considered as object or non-object (class affiliation) [15]. Perlin noise assigns gradient vectors at lattice points and interpolates between these points using a fade function [14, 16, 17].

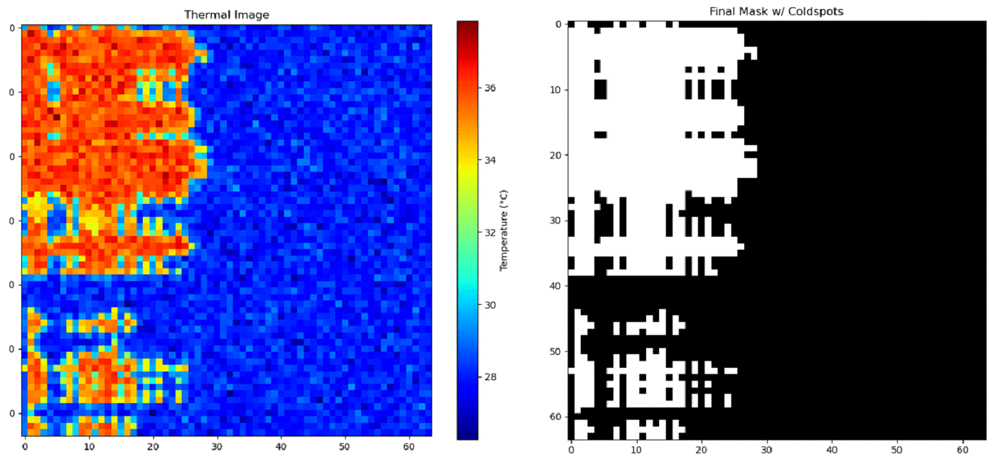

Fig. 10. Perlin/Simplex noise object generation and detection

These shapes are mathematically smooth and differentiable. Noise within these generated objects is coherent, guaranteeing smooth transitions in thermal values between neighboring pixels. In Perlin fields, there are some directional grid-like bias artifacts, and it is not computationally optimized. Simplex noise is an optimized version of Perlin noise where a simplex lattice is used (triangles in 2D) and has fewer grid artifacts. The method allows for easy configuration of the roughness of the generated shapes, their size, and their connectivity properties. Fig. 10 shows examples of Perlin noise-generated objects and the result from applying the object detection algorithm.

6. CONCLUSIONS

In this work, we have presented a developed cellular automata algorithm for infrared object detection. We performed statistical evaluations for the performance and noise resilience of the developed software module and showed the results as a set of 3D histograms. We proposed an optimization numerical criterion that can be used to select the object detection algorithm's tuning parameters. Proposed was the utilization of Perlin noise as a means for generating test thermogram datasets. Additionally, the algorithm was subjected to the temperature modulation phenomenon. The developed algorithm showed comparable performance to the benchmark algorithms but exceeded their resilience to temperature modulation.

ACKNOWLEDGMENT

This research is supported by the Bulgarian Ministry of Education and Science under the National Program "Young Scientists and Postdoctoral Students - 2".

REFERENCES

[1] A. BANULS, A. MANDOW, R. VÁZQUEZ-MARTÍN AND ET, AL., Object Detection from Thermal Infrared and Visible Light Cameras in Search and Rescue Scenes (2020) in: IEEE International Symposium on Safety, Security, and Rescue Robotics (SSRR), 4-6 November 2020, 380-386, online: https://doi.org/10.1109/SSRR50563.2020.9292593.

[2] J. LI AND J. YE, Edge-YOLO: Lightweight Infrared Object Detection Method Deployed on Edge Devices (2023) *J. Applied Sciences*, **13** (7) 4402, ISSN 2076-3417, online: https://doi.org/10.3390/app13074402.

[3] C. BAO, J. CAO, Q. HAO AND ET. AL., Dual-YOLO Architecture from Infrared and Visible Images for Object Detection (2023) *Sensors*, **23** (6) 2934, ISSN 1424-8220, online: https://doi.org/10.3390/s23062934.

[4] E. FENDRI, R. BOUKHRISS AND M. HAMMAMI, Fusion of Thermal Infrared and Visible Spectra for Robust Moving Object Detection (2017) *Pattern Analysis and Applications* **20** 10 907-926, online: https://doi.org/10.1007/s10044-017-0621-z.

[5] J. LIU, X. FAN, Z. HUANG AND ET. AL., Target-Aware Dual Adversarial Learning and a Multi-Scenario Multi-Modality Benchmark to Fuse Infrared and Visible for Object Detection (2022) in: Proceedings of the IEEE/CVF conference on computer vision and pattern recognition, June 2022, 5802-5811, online: https://doi.org/10.1109/CVPR52688.2022.00571.

[6] S. GAO, Y. CHENG AND Y. ZHAO, Method of Visual and Infrared Fusion for Moving Object Detection (2013) *Optics letters*, **38** (11) 1981-1983, ISSN 1539-4794, online: https://doi.org/10.1364/ol.38.001981.

[7] W. ZHAO, S. XIE, F. ZHAO AND ET. AL., Metafusion: Infrared and Visible Image Fusion via Meta-Feature Embedding from Object Detection (2023) in: Proceedings of the IEEE/CVF Conference on Computer Vision and Pattern Recognition, June 2023, 13955-13965, online: https://doi.org/10.1109/CVPR52729.2023.01341.

[8] X. WU, D. HONG AND J. CHANUSSOT, UIU-Net: U-Net in U-Net for Infrared Small Object Detection (2022) *IEEE Transactions on Image Processing*, **32** 364-376, online: https://doi.org/10.1109/TIP.2022.3228497.

[9] X. WU, D. HONG, Z. HUANG AND J. CHANUSSOT, Infrared Small Object Detection Using Deep Interactive U-Net (2022) *IEEE Geoscience and Remote Sensing Letters*, **19** 1-5, online: https://doi.org/10.1109/LGRS.2022.3218688.

[10] S. DU, B. ZHANG, P. ZHANG AND ET. AL., FA-YOLO: An Improved YOLO Model for Infrared Occlusion Object Detection under Confusing Background (2021) *Wireless*

Communications and Mobile Computing, **15,** 1-10, online: https://doi.org/10.1155/2021/1896029.
[11] EL BAF, T. BOUWMANS AND B. VACHON, Fuzzy Statistical Modeling of Dynamic Backgrounds for Moving Object Detection in Infrared Videos (2009) in: IEEE Computer Society Conference on Computer Vision and Pattern Recognition Workshops, June 2009, 60-65, online: https://doi.org/10.1109/CVPRW.2009.5204109.
[12] C. JIANG, H. REN, X. YE AND ET. AL., Object Detection from UAV Thermal Infrared Images and Videos Using YOLO Models (2022) *Int. Journal of Applied Earth Observation and Geoinformation*, **112**, online: https://doi.org/10.1016/j.jag.2022.102912.
[13] SH. LI, YONGJUN. LI, YAO. LI AND ET. AL., YOLO-FIRI: Improved YOLOv5 for Infrared Image Object Detection (2021) *IEEE access*, **99** 141861-141875, online: https://doi.org/10.1109/ACCESS.2021.3120870.
[14] D. EBERT, F. MUSGRAVE, D. PEACHEY AND ET. AL., *Texturing and modeling: a procedural approach* (3rd edition), Morgan Kaufmann Publishers, San Francisco (2003), ISBN 1-55860-8486.
[15] T. AKENINE-MÖLLER, E. HAINES AND N. HOFFMAN, *Real-time rendering* (3rd edition), A K Peters/CRC Press, New York (2019) ISBN: 978-1-3153-6545-9.
[16] J. HUGHES, A. VAN DAM, M. MCGUIRE AND ET. AL., Computer Graphics: Principles and Practice, Pearson Education Inc., Willard Ohio, USA (2014), ISBN 978-0-321-39952-6.
[17] K. PERLIN, An Image Synthesizer, ACM SIGGRAPH *Computer Graphics*, (1985) **19** (3), 287-296, online: https://doi.org/10.1145/325165.325247.

Received October 7, 2025